Uludağ University Journal of The Faculty of Engineering, Vol. 25, No. 1, 2020 RESEARCH

DOI: 10.17482/uumfd.597448

CORROSION BEHAVIOR OF ANNEALED STAINLESS STEEL MESH IN DIFFERENT ELECTROLYTES

Abdulcabbar YAVUZ [*]
Kaan KAPLAN [**]
Sitki AKTAS [***]

Received: 26.07.2019; revised: 10.04.2020; accepted: 16.04.2020

Abstract: This study aimed to investigate the corrosion behaviour of annealed stainless steel mesh. Thermal oxidation treatments were applied to steel mesh in a muffle furnace at 500 °C, 700 °C and 900 °C. Surface morphology of annealed and non-annealed stainless steel meshes was compared before and after polarization. The roughness of the steel surface was increased after heat-treatment. The corrosion properties of non-annealed and annealed steel were determined using linear sweep voltammetry. The corrosion behaviour of annealed stainless steel was examined utilizing a potentiostat in a 3.5 wt.% NaCl, 1 M H_2SO_4 and 1 M KOH electrolytes. The corrosion susceptibility of heat-treated stainless steel was more than that of non-heat treated stainless steel in alkaline electrolyte. While pitting corrosion of non-annealed and annealed stainless steel was different, corrosion potential and current of steel mesh without heat treatment were the same as the steel meshes annealed at 500 °C and 700 °C. Corrosion current and corrosion potential of non-annealed steel were the same as 500 °C annealed steel mesh in acidic medium.

Keywords: Corrosion, Stainless Steel, Heat-treatment, Thermal Oxidation

Paslanmaz Çelik Ağının Farklı Elektrolitler İçerisindeki Elektrokimyasal Davranışları

Öz: Bu çalışmanın amacı, tavlanmış paslanmaz çelik ağın korozyon davranışını incelemektir. Çelik ağa 500 °C, 700 °C ve 900 °C'de bir kül fırını içerisinde termal oksidasyon işlemleri uygulanmıştır. Tavlanmış ve tavlanmamış paslanmaz çelik ağların yüzey morfolojisi Elektrokimyasal polarizasyondan önce ve sonra karşılaştırılmıştır. Isıl işlemden sonra çelik yüzeyin pürüzlülüğü artmıştır. Tavlanmamış ve tavlanmış çeliğin korozyon özellikleri doğrusal tarama voltametrisi kullanılarak belirlenmiştir. Tavlı paslanmaz çeliğin korozyon davranışı, ağırlıkça % 3,5'lik NaCl, 1 M H_2SO_4 ve 1 M KOH elektrolitlerinde bir potansiyostat ile incelenmiştir. Isıl işlem görmüş paslanmaz çeliğin korozyon duyarlılığı, alkalin elektrolitte ısıl işlem görmemiş paslanmaz çeliğinkinden daha fazlaydı. Tavlanmamış ve tavlanmış paslanmaz çeliğin çukur korozyonu farklıyken, ısıl işlem uygulanmayan çelik ağın korozyon akımı ve korozyon potansiyeli 500 °C ve 700 °C'de tavlanan çelik ağlarla aynıydı. Tavlanmamış çeliğin korozyon akımı ve korozyon potansiyeli asidik ortamda 500 °C tavlanmış çelik ağınkiyle aynıydı.

Anahtar Kelimeler: Korozyon, Paslanmaz Çelik, Isıl İşlem, Isıl Oksidasyon

[*] Department of Metallurgical and Materials Engineering, Faculty of Engineering, Gaziantep University, Sehitkamil, 27310 Gaziantep, Turkey
[**] Department of Engineering Physics, Faculty of Engineering, Gaziantep University, Sehitkamil, 27310 Gaziantep, Turkey
[***] Mechanical Engineering, Giresun University, 28200 Giresun, Turkey
Corresponding Author: Abdulcabbar YAVUZ, ayavuz@gantep.edu.tr

1. INTRODUCTION

Stainless steel bulk materials have been used in various engineering applications because of their passivation behaviour and lack of environmental degradation (Hermas et al., 1995). Different types of stainless steel are used for appropriate demands. The main elements (after iron) in stainless steel is chromium and nickel. Generally, they are classified into four groups (duplex, austenitic, martensitic and ferritic) depending on their structure (Lo et al., 2009). It is known that the density of stainless steels is higher than some common engineering metals including aluminium, magnesium and titanium. However, specific strength of stainless steels is high and stainless steels possess high stiffness and high corrosion prevention (Eskandari et al., 2009). Surface treatments such as boronizing, nitriding and carburizing could change properties of stainless steel (Lindner et al., 2018). Electrochemical and physical properties of materials with the environment they are exposed could be related to the life of the material. Properties of materials could be tailored by surface treatments such as thermal and electrochemical treatments (Pippenger et al., 2019).

Metal oxides can be generated as they can be used in various applications including magnetic devices, catalysts, sensors, energy storage devices (Tartaj et al., 2011). Metal oxide/hydroxide have been used as corrosion prevention (Muhaffel and Cimenoglu, 2019; Zhang et al., 2018). Among metal oxides, iron-based oxides (FeO, Fe_2O_3 and Fe_3O_4) are of scientific and technological importance as they are inexpensive, highly abundant, generally stable and easy to prepare (Fiore et al., 2018).

Various preparation techniques including pyrolysis (Hassanien and Akl, 2018), chemical precipitation (Lassoued et al., 2018), solvo and hydrothermal (Köçkar et al., 2019), electrodeposition (Martinez et al., 2007), sol-gel (López-Sánchez et al., 2019) and RF sputtering (Lin et al., 1985) have been applied to obtain iron oxides. Surface morphology with various structure can be controlled by the formation route. Studies related to synthesis, structure and morphology of iron oxides were reported in the literature (Phul et al., 2019; Yu et al., 2018). In this study, iron oxide has been obtained by thermal oxidation and its corrosion behavior has been studied in acidic, neutral and alkaline electrolytes.

Metals/alloys can corrode because of their nature and formation process. Increasing annealing temperature cause easier oxidation (Zhou and Yang, 2004). Corrosion behaviors of different types of stainless steel have been studied (Bregliozzi et al., 2005; Pardo et al., 2008). Oxide forms of iron (FeO and Fe_2O_3) and chromium (Cr_2O_3) could occur on the outer surface of stainless steel with annealing temperature between 500 °C and 700 °C (Ferreira et al., 2001; Vesel et al., 2008). However, Cr_2O_3 coating could generally cover the stainless steel surface at the higher temperature (typically 800 °C) (Karlsson and Ribbing, 1982). The goal of this work is to measure the corrosion properties of heat-treated stainless steel mesh electrodes in NaCl, H_2SO_4 and KOH electrolyte.

2. EXPERIMENTAL

Potassium hydroxide (90 % purity, Tekkim), NaCl, (purity 99 %, Tekkim) and H_2SO_4 (purity 96 %, Merck) were used without purification. The stainless steel mesh was cut and each of them was 4 cm × 1 cm size. Thermal treatment of samples was performed at 500 °C, 700 °C and 900 °C for 30 minutes in a muffle furnace to produce oxidized surface. The corrosion properties of the annealed meshes were studied using a potentiostat measurement system (AMATEK, Princeton Applied Research, the USA). The results were checked by a different potentiostat (Gamry 1010E, the USA) to prove its reliability. Before the experiment, the samples were not ground and not washed. They were directly immersed in polarization electrolytes. Annealed samples of 1 cm × 1 cm were immersed in polarization solution for linear sweep voltammetry analysis. The polarization experiment was conducted in a three electrodes configuration of the electrochemical cell. Annealed samples were used as working electrodes. Ag/Ag^+ (saturated KCl solution) was the reference electrode. Platinum coated titanium mesh was a counter electrode. All

polarization tests were carried out at room temperature (20 ± 2 °C) Linear sweep voltammetry curves were obtained directly after the annealed samples were immersed in polarization solution. The polarization was started from the cathodic side to the direction of corrosion potential and anodic side. Images of the samples after polarization were taken by using Nikon LV150NL optical microscope.

3. RESULTS AND DISCUSSION

Stainless steel meshes were annealed in a muffle furnace and then transferred into the different electrolyte to measure their corrosion current and potential. The image of stainless steel mesh before annealing is given in Figure 1a. The surface of the non-annealed steel mesh was metallic shiny and smooth. After annealing at 300 °C, the colour of the stainless steel electrode was not shiny and changed to black as shown in Figure 1b. The surface colour of 500 °C annealed steel mesh was similar to that of 300 °C annealed steel mesh presented in Figure 1c. However, the surface of the steel mesh annealed at 800 °C was changed significantly (see Figure 1d). Heat treatment could cause different surface characteristics.

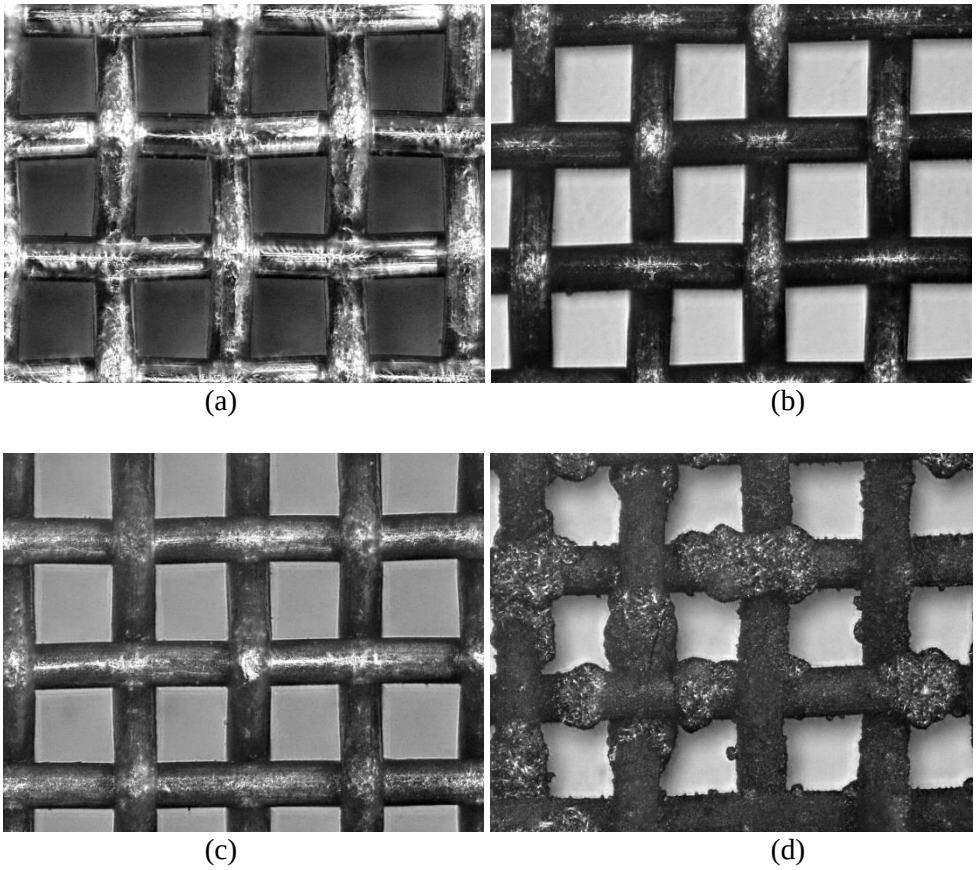

Figure 1:
Images of steel mesh electrode a) without heat treatments; b) annealed at 500 °C; c) annealed at 700 °C and; c) annealed at 900 °C. Images were magnified 100×

Thermal oxidation of an alloy could create metal oxide layers. Heat treatment of stainless steel could form oxide layers of chromium and iron. Fe_2O_3 and Cr_2O_3 layers are most likely

surface coating after annealing of stainless steel at high temperatures (Hamadou et al., 2010). It has been reported that Fe_2O_3 itself is formed on the surface of stainless steel up to around 400 °C. When the temperature is higher than 800 °C, the outer surface is generally Cr_2O_3 as it was studied in detail (Karlsson and Ribbing, 1982). The surface of stainless steel consists of both at the temperature between 400 °C and 800 °C. Therefore, the outer surface of stainless steel mesh annealed at 500 °C (Figure 1b) and 700 °C (Figure 1c) is a combination of Fe_2O_3 and Cr_2O_3. However, the surface of the steel mesh annealed at 900 °C (Figure 1d) has mainly Cr_2O_3. Heat-treated steel mesh was transferred to a different environment (acidic, alkaline and neutral) to characterize their corrosion behaviour and these results were compared with corrosion behaviour of non-annealed steel mesh.

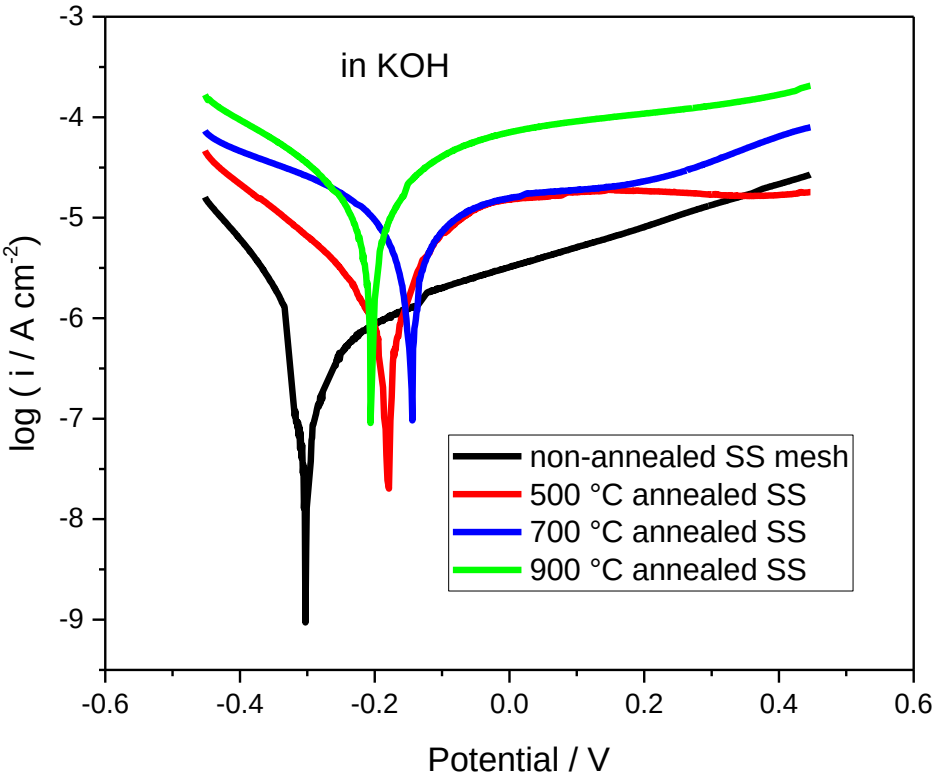

Figure 2:
Linear sweep voltammetry of non-annealed and annealed steel mesh in 1 M KOH electrolyte.

Annealed steel mesh was immersed in alkaline (1 M KOH) solution and linear sweep voltammetry technique were applied to investigate its corrosion behaviours. Figure 2 illustrates Tafel plot of non-annealed and annealed stainless steel meshes. Corrosion current of non-annealed mesh was increased from 0.4 µA cm^{-2} to 2.5 µA cm^{-2} after annealing at 500 °C. Corrosion current of non-annealed and annealed steels in KOH electrolyte is tabulated in Table 1. Corrosion current of 700 °C annealed steel even increased to 7.9 µA cm^{-2}. Corrosion current is directly proportional to the corrosion rate. As annealing temperature of stainless steel mesh increases, corrosion current (and corrosion rate) increases in alkaline electrolyte. Non-annealed stainless steel is about six and twenty times less electroactive than 500 °C and 700 °C annealed stainless steel mesh. This means that oxide forms of iron are more active than bare iron in alkaline solution. Therefore iron oxide-based electrodes in alkaline electrolyte could be used in electrochemical applications such as

energy storage devices (Du et al., 2009; Liu et al., 2016) and hydrogen evolution reaction (Askari et al., 2019).

Table 1: corrosion current (i_{corr}) values of non-annealed and annealed steel mesh in the different electrolyte.

	In KOH	In NaCl	In H_2SO_4
Non-annealed	0.4 μA cm^{-2}	2.5 μA cm^{-2}	2.5 mA cm^{-2}
500 °C annealed	2.5 μA cm^{-2}	2.3 μA cm^{-2}	2.4 mA cm^{-2}
700 °C annealed	7.9 μA cm^{-2}	2.2 μA cm^{-2}	1.6 mA cm^{-2}
900 °C annealed	25 μA cm^{-2}	26 μA cm^{-2}	1.2 mA cm^{-2}

Annealing temperature also increased the corrosion potential of stainless steel. While the corrosion potential of non-heated steel mesh was -0.30 V, that of 500 °C and 700 °C annealed stainless steel mesh was -0.17 V and -0.12 V, respectively. It is shown that Fe_2O_3 surface increases the rate of corrosion. Corrosion potential of 900 °C annealed steel mesh did not follow the same trend because the surface of 900 °C annealed steel mesh mainly consists of Cr_2O_3. Corrosion potential of Cr_2O_3 coated stainless steel was -0.20 V. However, corrosion current of 900 °C annealed steel mesh was much greater than that of 500 °C and 700 °C annealed stainless steel mesh and these results show that Cr_2O_3 coated steel can be more active in alkaline media. The corrosion rate of Cr_2O_3 coated steel is more than 60 times greater than that of bare steel in alkaline media as corrosion current of non-annealed steel was 0.4 μA cm^{-2} and corrosion rate of 900 °C annealed steel mesh was 25 μA cm^{-2}. 900 °C annealed steel mesh (photographed in Figure 3) was polarized in alkaline media utilizing linear sweep voltammetry and its surface was not changed significantly as shown in Figure 3b.

Table 2: corrosion potential (E_{corr}) values of non-annealed and annealed steel mesh in the different electrolyte.

	In KOH	In NaCl	In H_2SO_4
Non-annealed	-0.30 V	-0.39 V	-0.40 V
500 °C annealed	-0.17 V	-0.39 V	-0.40 V
700 °C annealed	-0.12 V	-0.39 V	-0.37 V
900 °C annealed	-0.20 V	-0.35 V	-0.35 V

Corrosion behaviour of steel generally was investigated in NaCl solution (Devikala et al., 2019; Yang et al., 2018). Stainless steel mesh electrodes were immersed in 3 wt. % NaCl solution. Linear sweep voltammetry for stainless steel mesh electrode in NaCl solution is presented in Figure 4. Black line of Figure 4 is the Tafel plot of non-annealed steel mesh in NaCl solution. Corrosion potential of non-annealed steel mesh was -0.39 V. The value of corrosion potential of 500 °C and 700 °C annealed steel mesh (-0.39 V) was the same as that of non-annealed steel mesh. The main difference between annealed steel mesh (at 500 °C and 700 °C) and non-annealed steel mesh was pitting corrosion potential. Pitting corrosion (sudden anodic increase) of non-annealed stainless was started at around +0.1 V (see black line of Figure 4). However, an anodic increase of annealed steel directly started after corrosion potential of -0.39 V. No passive behaviour of annealed stainless steel (at 500 °C and 700 °C) was observed.

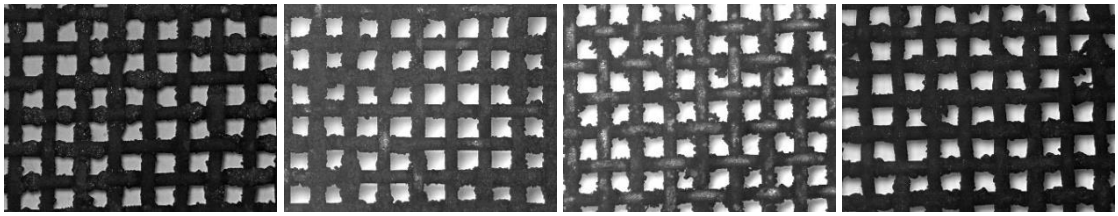

(a) (b) (c) (d)

Figure 3:

Images of a) polarized steel mesh annealed at 900 °C; b) polarized mesh in KOH; c) polarized mesh in NaCl and; d) polarized mesh in H_2SO_4

As it was indicated before, surface coating of stainless steel after annealing is the mixture of iron oxide and chromium oxide. Corrosion current density of bare stainless steel (2.5 µA cm^{-2}) was close to that of Fe_2O_3 and Cr_2O_3 coated stainless steel annealed at 500 °C and 700 °C. However, corrosion current density of (26 µA cm^{-2}) was more than ten times greater than non-annealed stainless steel (2.5 µA cm^{-2}) due to coated Cr_2O_3 surface. The surface area of steel (Figure 3a) was increased when the steel was heated at 900 °C (see Figure 3c). The colour of homogenous electrolyte containing NaCl salt (left photo of Figure 4 inlet) became brownish after polarization experiment (right photo of Figure 4 inlet) given in Figure 4 because iron was oxidized to its ionic forms and dissolved in aqueous media.

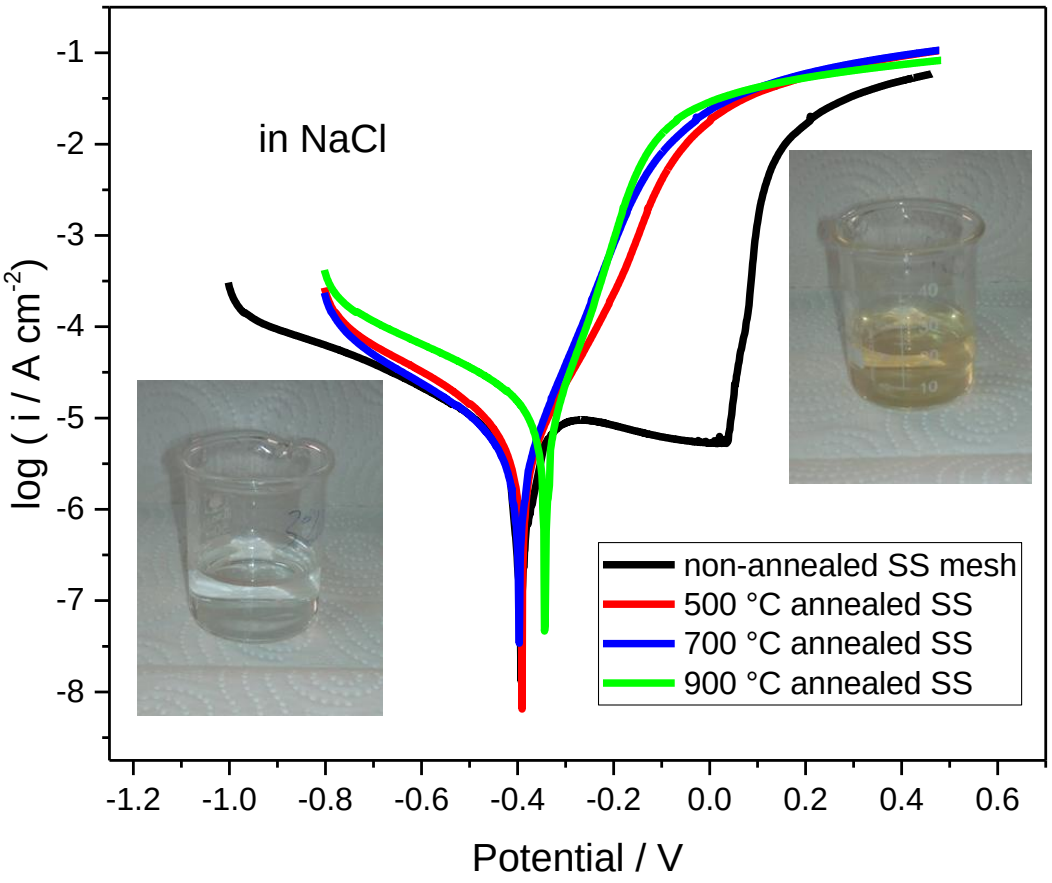

Figure 4:

Tafel plot of non-annealed and annealed steel mesh in 3 wt.% NaCl solution

The corrosion rate of steel in acidic medium is quite high and investigated in the literature (Biswas et al., 2018; Hassan et al., 2019; Saad et al., 2018) and generally, inhibitors have been suggested to decrease the corrosion rate of stainless steel. Stainless steel mesh electrodes were immersed in 1 M H_2SO_4 solution. Polarization of stainless steel mesh electrode in H_2SO_4 solution is presented in Figure 5. The Tafel plot of non-annealed steel mesh in H_2SO_4 solution is presented in Figure 5. Corrosion potential of non-annealed steel and 500 °C annealed steel mesh was the same (-0.40 V) in acidic medium. All corrosion potential of non-annealed and annealed (at a different temperature) is presented in Table 2. Corrosion characteristic of non-annealed and 500 °C annealed steel mesh is the same as their current decrease at around -0.4 V is the same as iron dominates the corrosion behaviour of thin iron oxide solution. However, high annealed temperature cause a positive shift in potential value and a negative shift in current value indicating that electroactivity of 500 °C and 700 °C annealed steel meshes is lower than that of non-heated steel mesh. Corrosion current of non-annealed and 500 °C annealed steel started to decrease at around -0.3 V after Tafel area. However, corrosion current of 700 °C and 900 °C annealed steel mesh continued to increase.

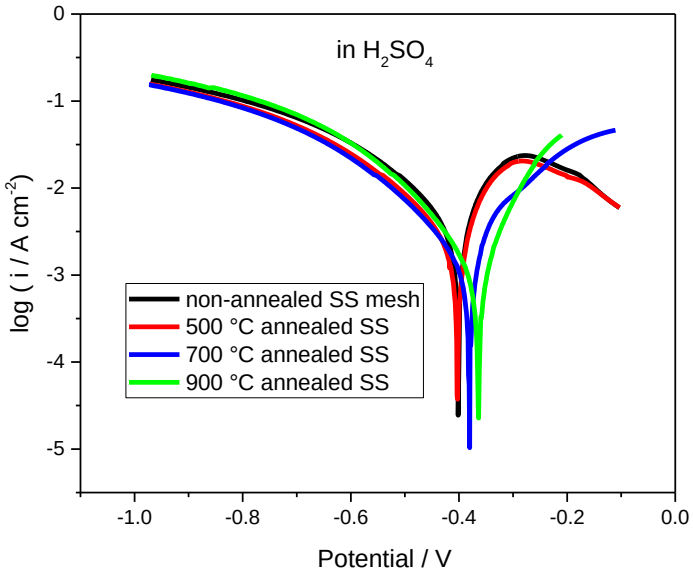

Figure 5:
Linear sweep polarization of non-annealed and annealed steel mesh in H_2SO_4

4. CONCLUSION

Stainless steel meshes were heated at 500 °C, 700 °C and 900 °C in a muffle furnace to obtain an oxidized surface. The surface of the non-annealed steel mesh became rougher after annealing. Increasing annealing temperature caused a darker surface. Steel meshes were transferred into the different electrolyte (acidic, alkaline and neutral) for corrosion studies. Corrosion behaviour of annealed stainless steel mesh was compared with that of non-annealed steel mesh. Corrosion current of annealed stainless steel increases in an alkaline electrolyte (1 M KOH) when annealing temperature of stainless steel mesh increases. The corrosion potential of stainless steel increased upon increasing the annealing temperature. Therefore, annealed stainless steel (oxidized form of iron) is more active than non-annealed stainless steel (iron) in alkaline electrolyte.

Corrosion behaviour of stainless steel mesh electrodes was investigated in 3 wt.% NaCl electrolyte utilizing linear sweep voltammetry technique. The value of corrosion potential and corrosion current of non-annealed steel mesh was the same as that of 500 °C and 700 °C annealed

steel mesh but pitting corrosion potential of them are different. The colour of polarization electrolyte containing NaCl salt was changed to brownish after linear sweep voltammetry (corrosion) experiment. Corrosion behaviour (corrosion current and corrosion potential) of non-annealed steel and 500 °C annealed steel mesh was the same in acidic medium. The potential and current value of stainless steel meshes obtained at high annealing temperature were shifted to more active sides. The research illustrates that heat-treated stainless steel (without surface removal) can be used in acidic media as corrosion behaviour of stainless steel has similar behaviour with and without heat treatment. However, corrosion susceptibility of heat-treated stainless steel is higher than non-heated stainless steel in alkaline and neutral environment.

ACKNOWLEDGEMENT

Kaan Kaplan would like to thank the Council of Higher Education for the YÖK 100/2000 doctoral scholarship. AY and KK are grateful to Gaziantep University BAP for financial support (MF.DT.19.16).

REFERENCES

1. Askari, M. B., Beheshti-Marnani, A., Seifi, M., Rozati, S. M., & Salarizadeh, P. (2019). Fe3O4@ MoS2/RGO as an effective nano-electrocatalyst toward electrochemical hydrogen evolution reaction and methanol oxidation in two settings for fuel cell application. *Journal of Colloid and Interface Science*, *537*, 186–196. doi.org/10.1016/j.jcis.2018.11.019

2. Biswas, A., Mourya, P., Mondal, D., Pal, S., & Udayabhanu, G. (2018). Grafting effect of gum acacia on mild steel corrosion in acidic medium: Gravimetric and electrochemical study. *Journal of Molecular Liquids*, *251*, 470–479. doi.org/10.1016/j.molliq.2017.12.087

3. Bregliozzi, G., Di Schino, A., Ahmed, S.-U., Kenny, J. M., & Haefke, H. (2005). Cavitation wear behaviour of austenitic stainless steels with different grain sizes. *Wear*, *258*(1–4), 503–510. doi.org/10.1016/j.wear.2004.03.024

4. Devikala, S., Kamaraj, P., Arthanareeswari, M., & Patel, M. B. (2019). Green corrosion inhibition of mild steel by aqueous Allium sativum extract in 3.5% NaCl. *Materials Today: Proceedings*, *14*, 580–589. doi.org/10.1016/j.matpr.2019.04.182

5. Du, X., Wang, C., Chen, M., Jiao, Y., & Wang, J. (2009). Electrochemical performances of nanoparticle Fe3O4/activated carbon supercapacitor using KOH electrolyte solution. *The Journal of Physical Chemistry C*, *113*(6), 2643–2646. doi.org/10.1021/jp8088269

6. Eskandari, M., Najafizadeh, A., Kermanpur, A., & Karimi, M. (2009). Potential application of nanocrystalline 301 austenitic stainless steel in lightweight vehicle structures. *Materials & Design*, *30*(9), 3869–3872. doi.org/10.1016/j.matdes.2009.03.043

7. Ferreira, M. G. S., Hakiki, N. E., Goodlet, G., Faty, S., Simoes, A. M. P., & Belo, M. D. C. (2001). Influence of the temperature of film formation on the electronic structure of oxide films formed on 304 stainless steel. *Electrochimica Acta*, *46*(24–25), 3767–3776. doi.org/10.1016/S0013-4686(01)00658-2

8. Fiore, M., Longoni, G., Santangelo, S., Pantò, F., Stelitano, S., Frontera, P., Antonucci, P., & Ruffo, R. (2018). Electrochemical characterization of highly abundant, low cost iron (III) oxide as anode material for sodium-ion rechargeable batteries. *Electrochimica Acta*, *269*, 367–377. doi.org/10.1016/j.electacta.2018.02.161

9. Hamadou, L., Kadri, A., & Benbrahim, N. (2010). Impedance investigation of thermally formed oxide films on AISI 304L stainless steel. *Corrosion Science*, *52*(3), 859–864. doi.org/10.1016/j.corsci.2009.11.004

10. Hassan, N., Ali, S. M., Ebrahim, A., & El-Adwy, H. (2019). Performance evaluation and optimization of Camellia sinensis extract as green corrosion inhibitor for mild steel in acidic medium. *Materials Research Express*, *6*(8), 0865c7. doi.org/10.1088/2053-1591/ab2376

11. Hassanien, A. S., & Akl, A. A. (2018). Optical characteristics of iron oxide thin films prepared by spray pyrolysis technique at different substrate temperatures. *Applied Physics A*, *124*(11), 752. doi.org/10.1007/s00339-018-2180-6

12. Hermas, A. A., Ogura, K., Takagi, S., & Adachi, T. (1995). Effects of alloying additions on corrosion and passivation behaviors of type 304 stainless steel. *Corrosion*, *51*(1), 3–10. doi.org/10.5006/1.3293575

13. Karlsson, B., & Ribbing, C. G. (1982). Optical constants and spectral selectivity of stainless steel and its oxides. *Journal of Applied Physics*, *53*(9), 6340–6346. https://doi.org/10.1063/1.331503

14. Köçkar, H., Karaagac, O., & Özel, F. (2019). Effects of biocompatible surfactants on structural and corresponding magnetic properties of iron oxide nanoparticles coated by hydrothermal process. *Journal of Magnetism and Magnetic Materials*, *474*, 332–336. doi.org/10.1016/j.jmmm.2018.11.053

15. Lassoued, A., Lassoued, M. S., Dkhil, B., Ammar, S., & Gadri, A. (2018). Synthesis, structural, morphological, optical and magnetic characterization of iron oxide (α-Fe2O3) nanoparticles by precipitation method: effect of varying the nature of precursor. *Physica E: Low-Dimensional Systems and Nanostructures*, *97*, 328–334. doi.org/10.1016/j.physe.2017.12.004

16. Lin, J., Silvertsen, J., & Judy, J. (1985). Properties of RF sputtered iron oxide thin films with CoCr and Nb as dopants. *IEEE Transactions on Magnetics*, *21*(5), 1462–1464. doi.org/10.1109/tmag.1985.1063953

17. Lindner, T., Kutschmann, P., Löbel, M., & Lampke, T. (2018). Hardening of HVOF-sprayed austenitic stainless-steel coatings by gas nitriding. *Coatings*, *8*(10), 348. doi.org/10.3390/coatings8100348

18. Liu, L., Lang, J., Zhang, P., Hu, B., & Yan, X. (2016). Facile synthesis of Fe2O3 nano-dots@ nitrogen-doped graphene for supercapacitor electrode with ultralong cycle life in KOH electrolyte. *ACS Applied Materials & Interfaces*, *8*(14), 9335–9344. doi.org/10.1021/acsami.6b00225

19. Lo, K. H., Shek, C. H., & Lai, J. K. L. (2009). Recent developments in stainless steels. *Materials Science and Engineering: R: Reports*, *65*(4–6), 39–104. doi.org/10.1016/j.mser.2009.03.001

20. López-Sánchez, J., Serrano, A., del Campo, A., Abuín, M., Salas-Colera, E., Muñoz-Noval, A., Castro, G. R., de la Figuera, J., Marco, J. F., & Marín, P. (2019). Self-assembly of iron oxide precursor micelles driven by magnetic stirring time in sol–gel coatings. *RSC Advances*, *9*(31), 17571–17580. doi.org/10.1016/j.mser.2009.03.001

21. Martinez, L., Leinen, D., Martin, F., Gabas, M., Ramos-Barrado, J. R., Quagliata, E., & Dalchiele, E. A. (2007). Electrochemical growth of diverse iron oxide (Fe3O4, α-FeOOH, and γ-FeOOH) thin films by electrodeposition potential tuning. *Journal of the Electrochemical Society*, *154*(3), D126–D133. doi.org/10.1149/1.2424416

22. Muhaffel, F., & Cimenoglu, H. (2019). Development of corrosion and wear resistant micro-arc oxidation coating on a magnesium alloy. *Surface and Coatings Technology*, *357*, 822–832. doi.org/10.1016/j.surfcoat.2018.10.089

23. Pardo, A., Merino, M. C., Coy, A. E., Viejo, F., Arrabal, R., & Matykina, E. (2008). Pitting corrosion behaviour of austenitic stainless steels–combining effects of Mn and Mo additions. *Corrosion Science*, *50*(6), 1796–1806. doi.org/10.1016/j.corsci.2008.04.005

24. Phul, R., Shrivastava, V., Farooq, U., Sardar, M., Kalam, A., Al-Sehemi, A. G., & Ahmad, T. (2019). One pot synthesis and surface modification of mesoporous iron oxide nanoparticles. *Nano-Structures & Nano-Objects*, *19*, 100343. doi.org/10.1016/j.nanoso.2019.100343

25. Pippenger, B. E., Rottmar, M., Kopf, B. S., Stübinger, S., Dalla Torre, F. H., Berner, S., & Maniura-Weber, K. (2019). Surface modification of ultrafine-grained titanium: Influence on mechanical properties, cytocompatibility, and osseointegration potential. *Clinical Oral Implants Research*, *30*(1), 99–110. doi.org/10.1111/clr.13396

26. Saad, I. R., Abdel-Gaber, A. M., Younes, G. O., & Nsouli, B. (2018). Corrosion Inhibition of Mild Steel in Acidic Solutions Using 1, 2, 4-Triazolo [1, 5-a] pyrimidine. *Russian Journal of Applied Chemistry*, *91*(2), 245–252. doi.org/10.1134/S107042721802012X

27. Tartaj, P., Morales, M. P., Gonzalez-Carreño, T., Veintemillas-Verdaguer, S., & Serna, C. J. (2011). The iron oxides strike back: from biomedical applications to energy storage devices and photoelectrochemical water splitting. *Advanced Materials*, *23*(44), 5243–5249. doi.org/10.1002/adma.201101368

28. Vesel, A., Mozetic, M., Drenik, A., Hauptman, N., & Balat-Pichelin, M. (2008). High temperature oxidation of stainless steel AISI316L in air plasma. *Applied Surface Science*, *255*(5 PART 1), 1759–1765. https://doi.org/10.1016/j.apsusc.2008.06.017

29. Yang, J., Lu, Y., Guo, Z., Gu, J., & Gu, C. (2018). Corrosion behaviour of a quenched and partitioned medium carbon steel in 3.5 wt.% NaCl solution. *Corrosion Science*, *130*, 64–75. doi.org/10.1016/j.corsci.2017.10.027

30. Yu, L., Han, R., Sang, X., Liu, J., Thomas, M. P., Hudak, B. M., Patel, A., Page, K., & Guiton, B. S. (2018). Shell-induced Ostwald ripening: simultaneous structure, composition, and morphology transformations during the creation of hollow iron oxide nanocapsules. *ACS Nano*, *12*(9), 9051–9059. doi.org/10.1021/acsnano.8b02946

31. Zhang, G., Wu, L., Tang, A., Ma, Y., Song, G.-L., Zheng, D., Jiang, B., Atrens, A., & Pan, F. (2018). Active corrosion protection by a smart coating based on a MgAl-layered double hydroxide on a cerium-modified plasma electrolytic oxidation coating on Mg alloy AZ31. *Corrosion Science*, *139*, 370–382. doi.org/10.1016/j.corsci.2018.05.010

32. Zhou, G., & Yang, J. C. (2004). Temperature effects on the growth of oxide islands on Cu (1 1 0). *Applied Surface Science*, *222*(1–4), 357–364. doi.org/10.1016/j.apsusc.2003.09.008